Prompt fission neutron (PFN) emission in $^{252}Cf\,(SF)\;and\;^{235}U(n_{th},f)$ *reaction*

Zeynalov Sh. Sedyshev P., Sidorova O., Shvetsov V.

JINR-Joint Institute for Nuclear Research, Dubna, Russia

Wonder-2018, October 8-12

2. Motivation

The mechanism of PFN emission in fission plays important role in nuclear fission theory from the one hand and the information on PFN is highly demanded by nuclear power industry from the other hand.

Analysis of TKE measured in resonance neutron induced fission of ^{235}U revealed surprising fluctuation. The recent measurement of PFN multiplicity in ^{235}U resonances demonstrates fluctuations of PFN multiplicities to.

One of the interesting observation is the increasing $\bar{\nu}(A)$ from the heavy FF with increase of the excitation energy of fissioning system still has no clear explanation

In current report we presenting some preliminary results of measurement of PFN emission in thermal neutron induced fission of ^{235}U reaction as test of apparatus for resonance neutron induced fission of ^{235}U measurements foreseen to perform at IREN facility next year

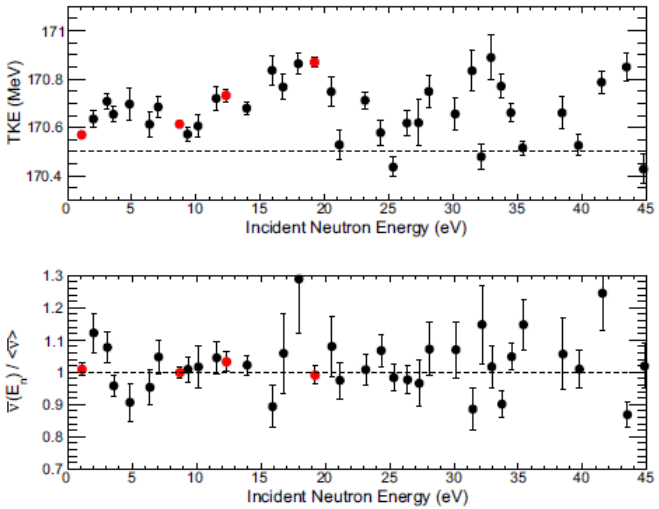

EPJ Web of Conferences **111**, 05001 (2016)
DOI: 10.1051/epjconf/201611105001

3. Experimental setup and data acquisition system.

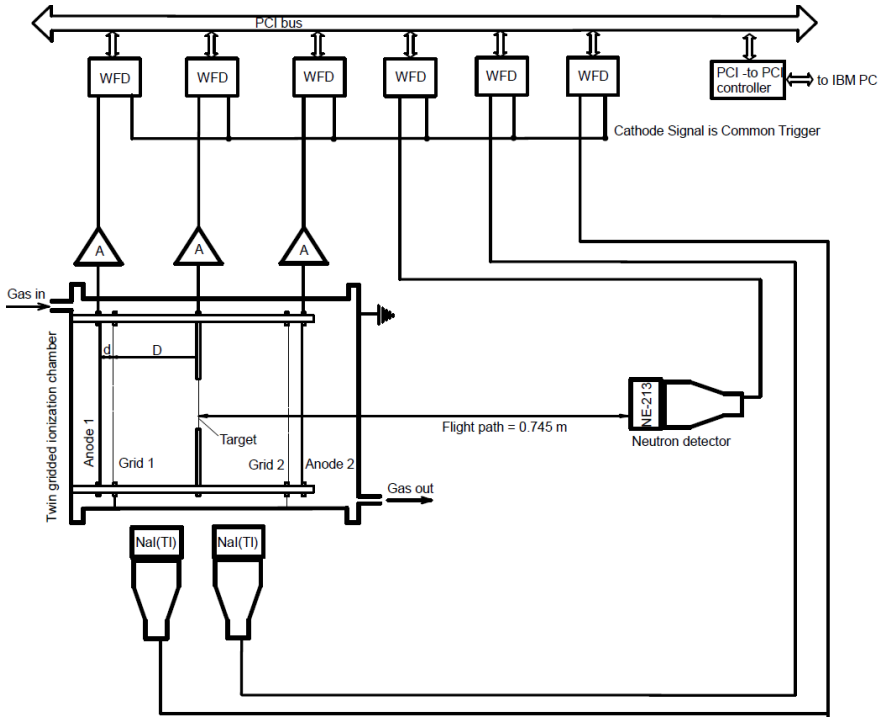

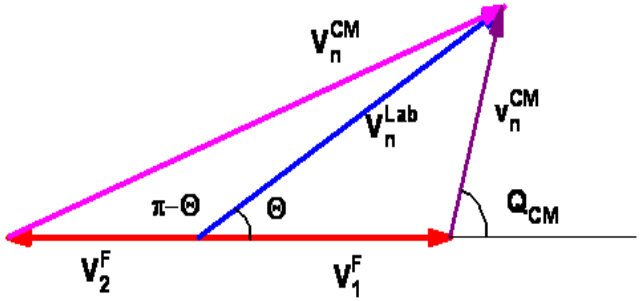

$$\bar{\nu}(A)=\frac{\int_0^\infty \nu(A,TKE)Y(A,TKE)dTKE}{\int_0^\infty Y(A,TKE)dTKE},\quad \bar{\nu}=\int_0^\infty \nu(A,TKE)Y(A,TKE)dTKEdA,\quad 200=\int_0^\infty Y(A,TKE)dTKEdA$$

$$\bar{\nu}(TKE)=\frac{\int_0^\infty \nu(A,TKE)Y(A,TKE)dA}{\int_0^\infty Y(A,TKE)dA},\quad \bar{\nu}=\int_0^\infty \nu(A,TKE)Y(A,TKE)dTKEdA,\quad 200=\int_0^\infty Y(A,TKE)dTKEdA$$

Adopted from C. Budtz-Jørgensen and H.-H. Knitter, *Nucl. Phys.*, A490, 307(1988) and modified with digital pulse processing apparatus

4. Digital Pulse Processing (DPP).

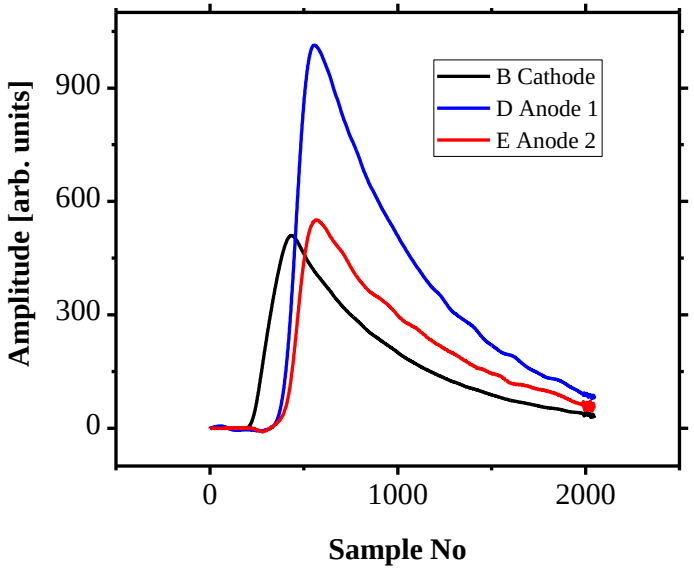

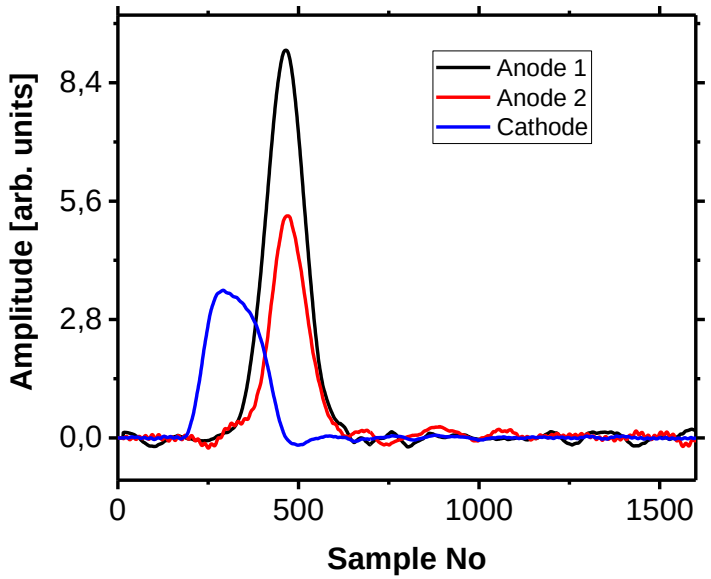

In our approach we have oversampled FF signals. The oversampling we used to increase the effective number of bits (ENOB) improving the signal representation. In practice the increase of ENOB realized automatically when signal passed through second order low pass filter :

$$V^1_{out}(t) = \int_0^\infty V_{in}(\xi) \bullet \exp(-\frac{(\xi - t)}{\tau}) d\xi,\ V^2_{out} = \int_0^\infty V^1_{out}(\xi) \bullet \exp(-\frac{(\xi - t)}{\tau}) d\xi$$

Improved signal presentation (left figure) facilitates numerical solution (differentiation) of the integral equation

$$V(t) = Const \bullet \int_0^t i(\xi) \exp(-\xi / \tau) d\xi$$

Solution of the equation is i(t) presented on the right figure for the cathode and two anode signals. In terms of familiar analog electronics the operation performed equivalent to differential filter on the input of spectroscopy amplifier (SA). To simulate integrating stage of the SA we implemented integration according to

$$V(t) = \int_0^t i(\xi) d\xi$$

The last operation, performed with two correlated anode waveforms, provides the pulse heights of FF.

5. Drift time determination of FF ionization

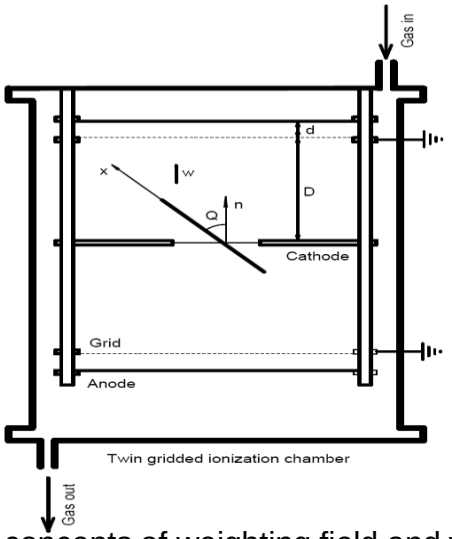

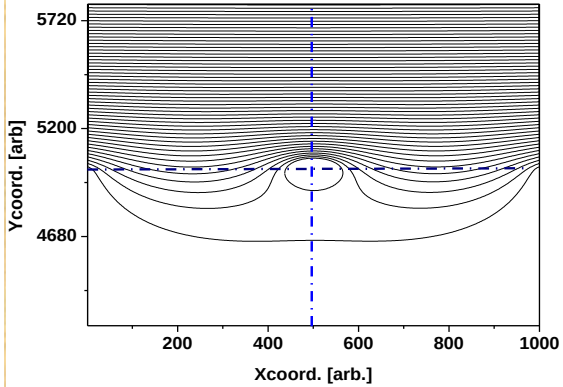

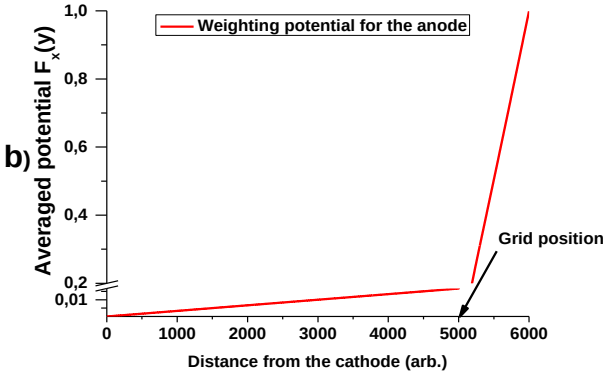

The concepts of weighting field and weighting potential states that the instantaneous current induced on a given electrode is equal to $i = q\bar{v}E_0$, where q is the charge of the carrier, $\bar{v}$ is its velocity, and E_0 is called the weighting field. Another way of stating the same principle is that the induced charge on the electrode is given by the product of the charge on the carrier multiplied by the difference in the weighting potential from the beginning to the end of the carrier path $Q = q\Delta\Phi$. The weighting potential as a function of position was found as the solution of the Laplace equation for the geometry of the detector with special boundary conditions. Evaluation of the drift time can be done if the weighting potential inside the sensitive volume of the chamber is calculated as shown in the above graphs. Using explicit functions for weighting potential one can find the following expression for drift time T for ionization charge density shifting from the origin to the anode:

$$T = \frac{D}{W} \bullet \left\{ (1 - \frac{\overline{X}}{D} \bullet \cos(\Theta)) + \frac{d}{2 \bullet D} \bullet (1 - \frac{\sigma}{1-\sigma} \bullet (1 - \frac{\overline{X}}{D} \cos(\Theta)) \right\},$$

where the meanings of d, D, Θ are clear from the sketch of the TBIC, ϭ is the grid inefficiency factor or it is the value of the average weighting potential at grid location, and X is the center for ionization charge distribution along the FF track. Parameter T for corresponding anode can be measured using the signal current waveform as follows

$$T = S / S_0, \text{ where } S = \int_0^{T_{\max}} i(t) * t dt, \; S_0 = \int_0^{T_{\max}} i(t) dt$$

6. FFs cos(Θ) evaluation

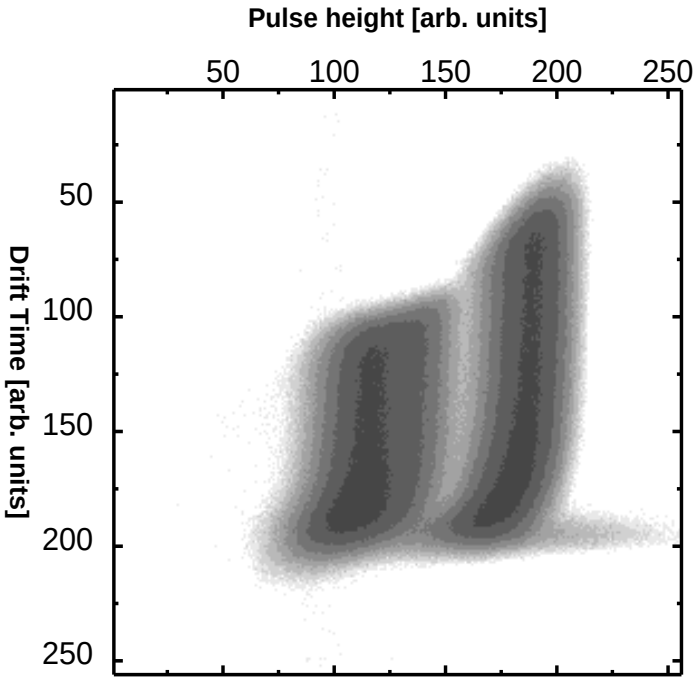

$$T = \frac{D}{W}\cdot\left\{(1-\frac{\overline{X}}{D}\cdot\cos(\Theta))+\frac{d}{2\cdot D}\cdot(1-\frac{\sigma}{1-\sigma}\cdot(1-\frac{\overline{X}}{D}\cdot\cos(\Theta))\right\}$$

$$\cos(\Theta) = \frac{T_{90}-T}{T_{90}-T_0} \qquad T_0 = T(\cos(\Theta)=1)$$

$$\mathrm{T}_{90} = T(\cos(\Theta)=0)$$

$$P_A^C = P_A/(1-\sigma(1-\frac{T}{T_{90}})\cdot(1+\frac{d}{2D}))$$

Cosines calculated from measured drift times T according to formulae above.

7. FFs pulse height correction for cos(Θ)

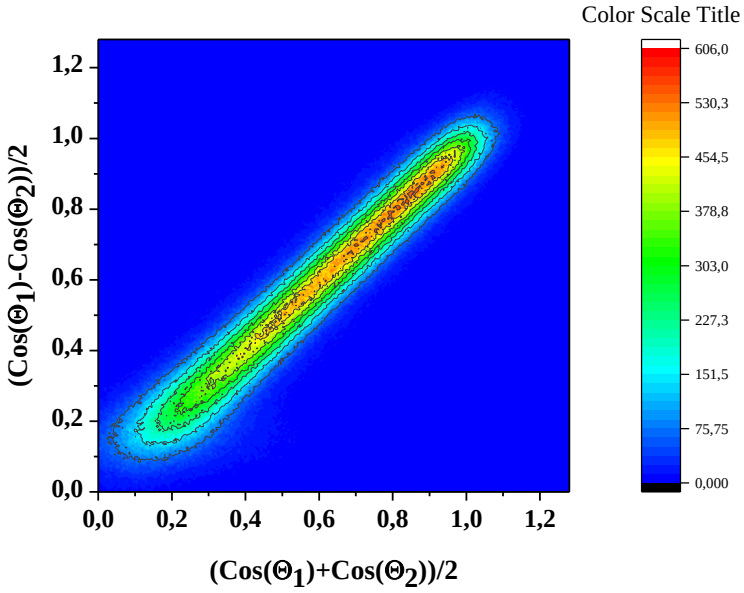

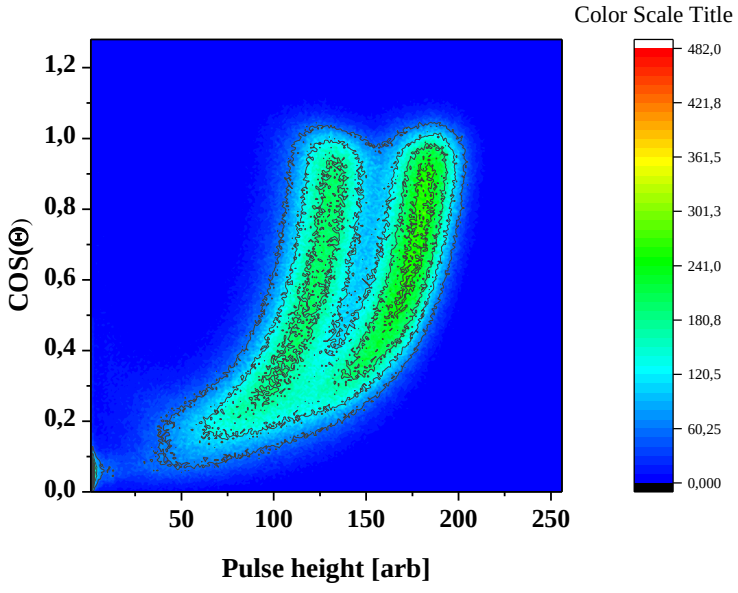

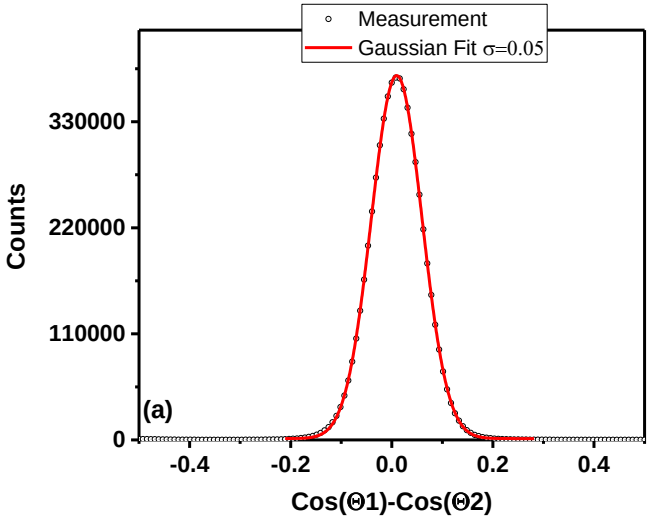

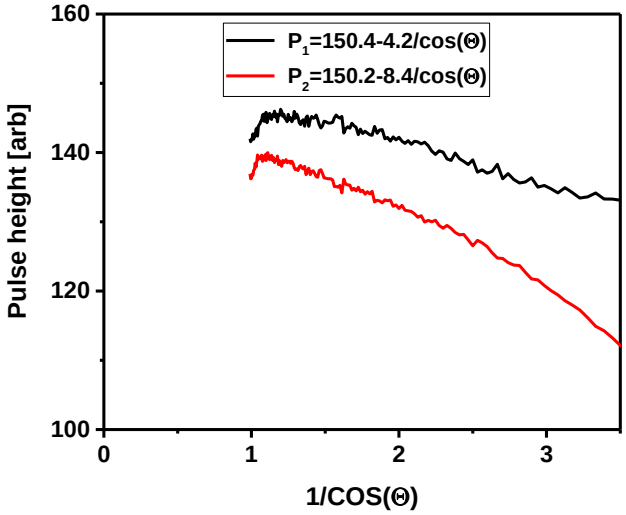

8. PHD correction

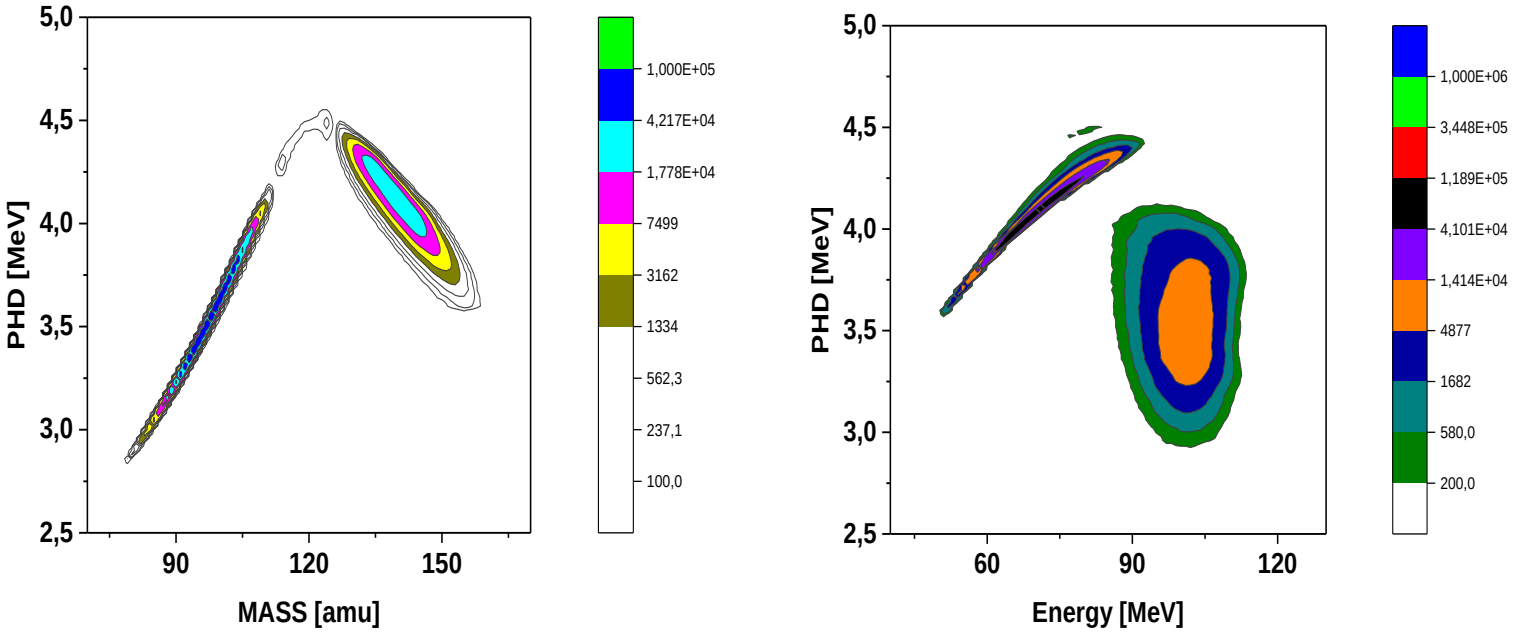

$$E = \alpha * PH + \beta + PHD(A_{post}, E_{post})$$

The correction for FF pulse height caused by momentum transfer to working gas atoms by FF (non ionizing collisions) during its deceleration – is called pulse height defect (PHD). The PHD depends on the FF mass and kinetic energy and was corrected in data analysis using parameterization presented above. Figures demonstrate PHD dependence on mass and kinetic energies of FFs, measured in $^{235}U(n_{th},ff)$ reaction investigation.

9. FF mass&energy distributions.

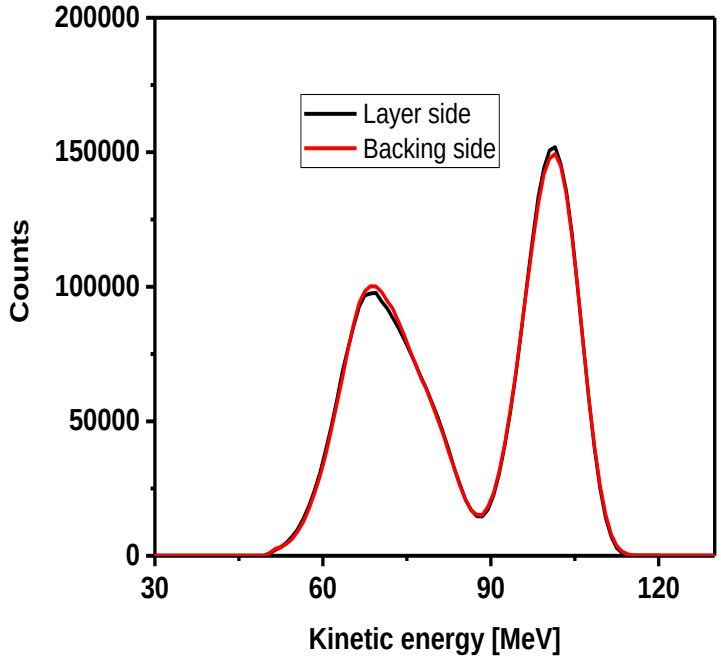

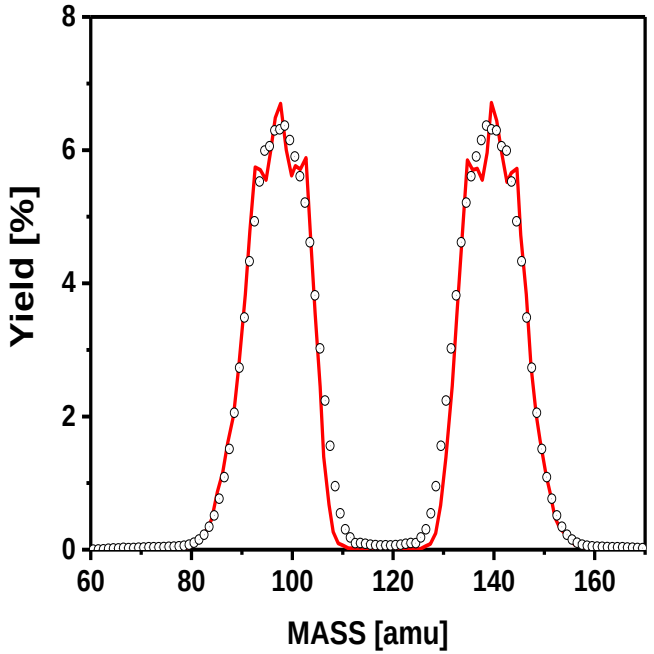

10. Constant fraction time marking for PFN TOF measurement

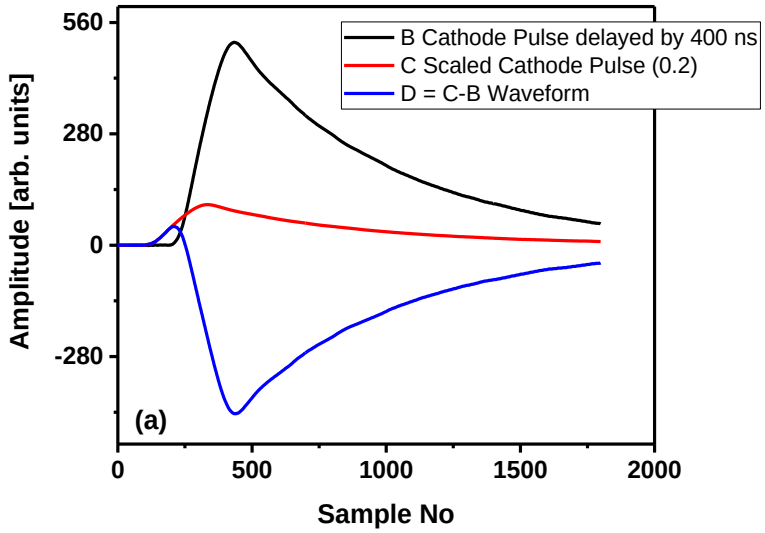

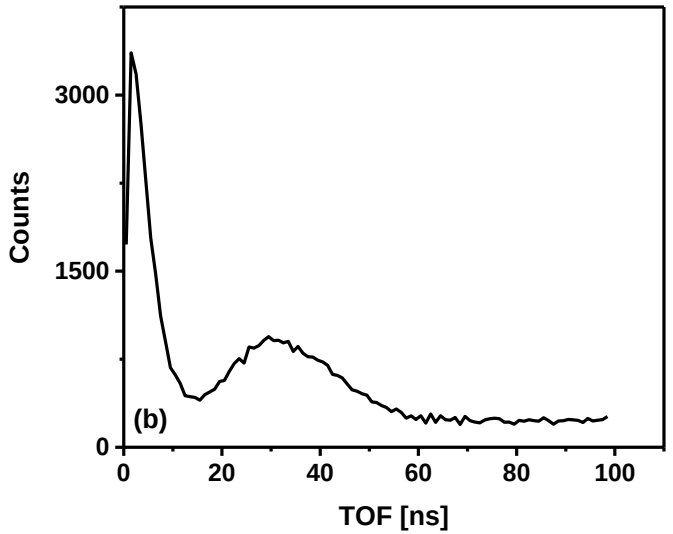

11. Neutron separation from gamma radiation

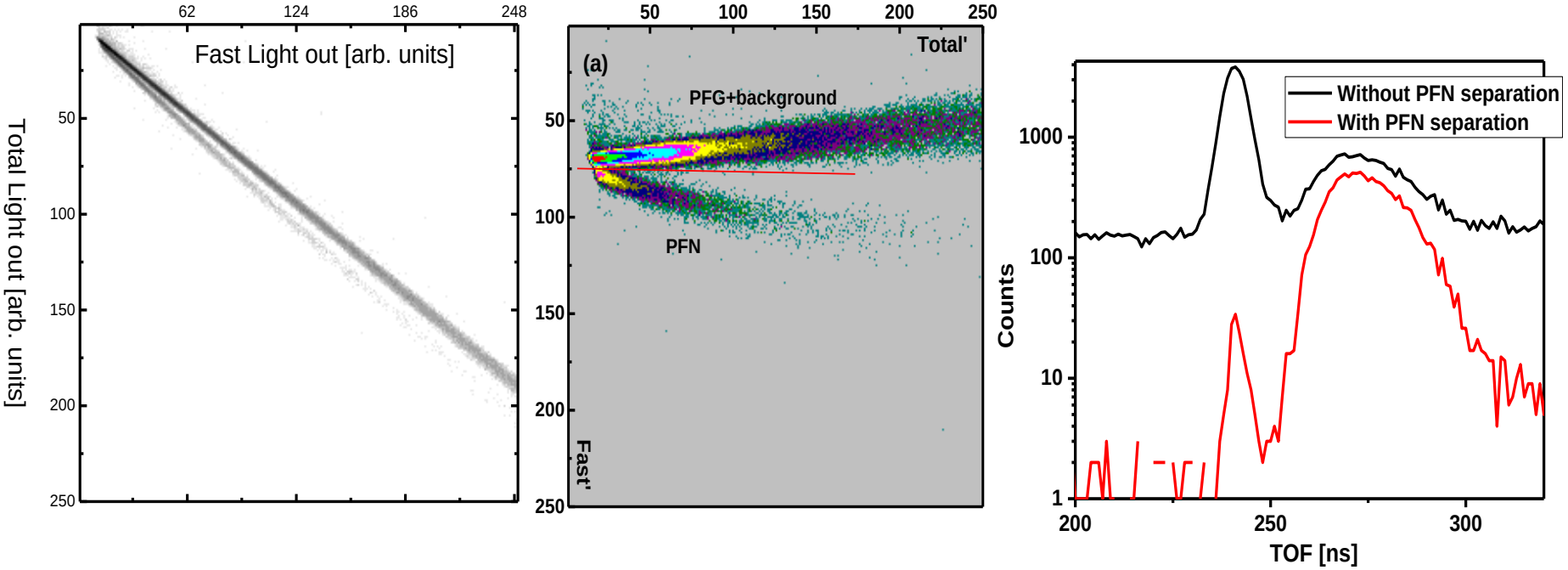

The two window algorithm (fast and total light output component) was implemented and resulted function *ND(Fast,Total)* was plotted on the upper and middle figs. demonstrates the function *ND(Fast,Total) i*n rotated according to equation

$$F' = F \bullet \cos(\Omega) + T \bullet \sin(\Omega), T' = S \bullet \{-F \bullet \sin(\Omega) + T \bullet \cos(\Omega)\}$$

,where Ω – is axes rotation angle and S>1 – is the scaling factor. Red line in the middle figure is PFN-PFG separation line . Lower figure demonstrates the TOF distribution before and after PFN separation.

12. PFN angular distribution measurement

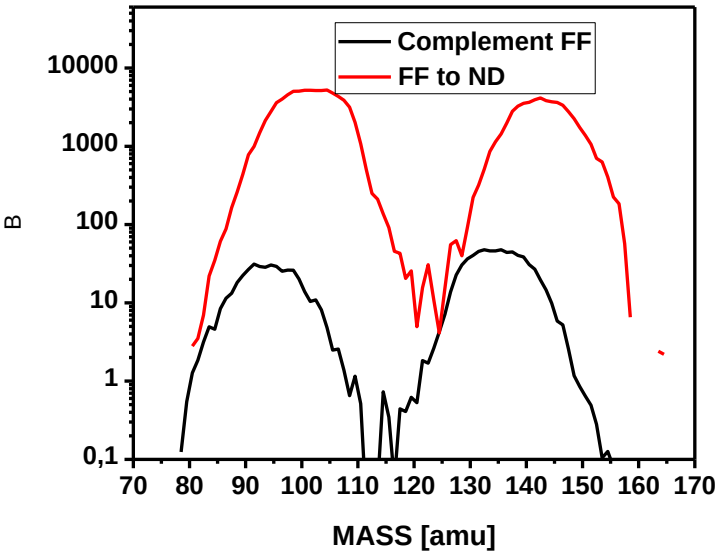

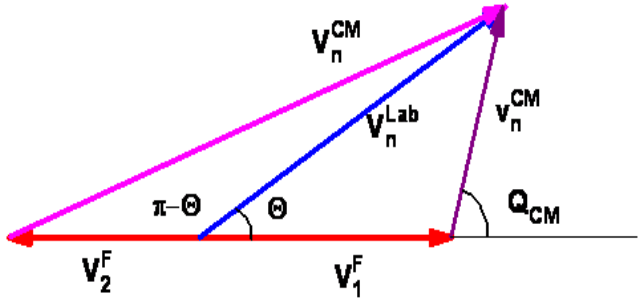

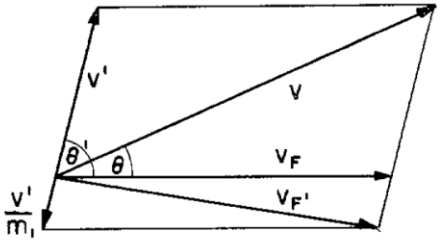

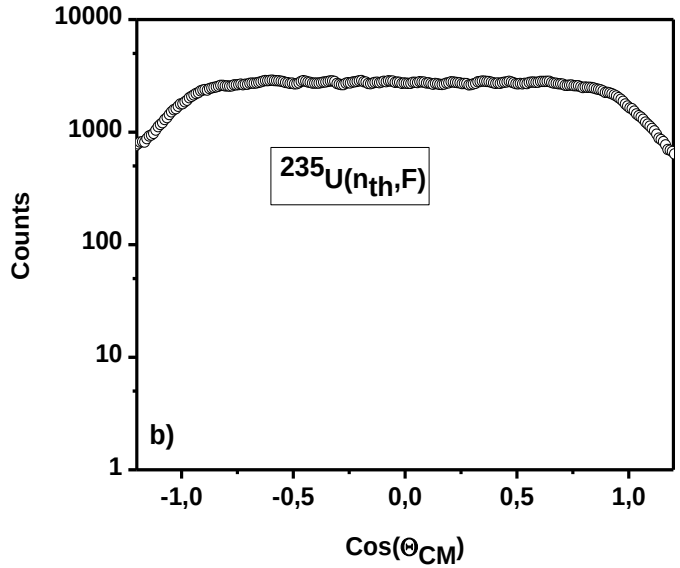

Correction for FF recoil according to
Nucl. Instrum. and Meth., 115 (1974) 99

$$W_x = 1,\ W_y = \exp(E_{CM}^x - E_{CM}^y)$$

C. Budtz-Jorgensen and H.-H. Knitter, Nucl. Phys., A490, 307 (1988) for PFN emission from complementary FF

13. ND efficiency evaluation

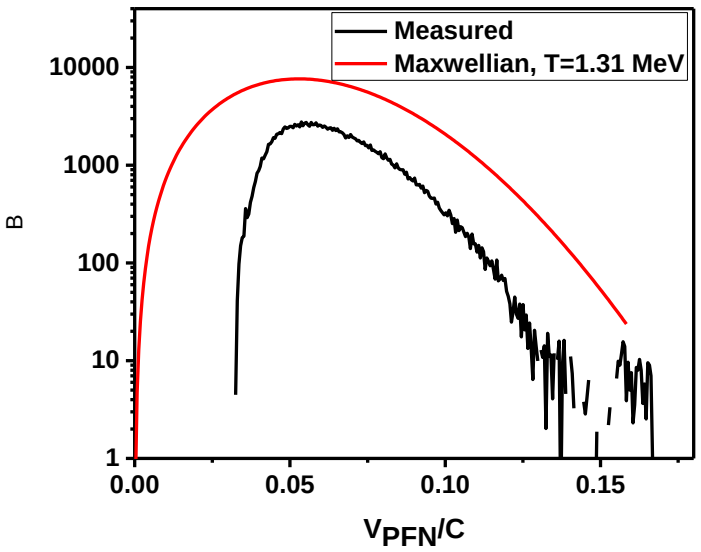

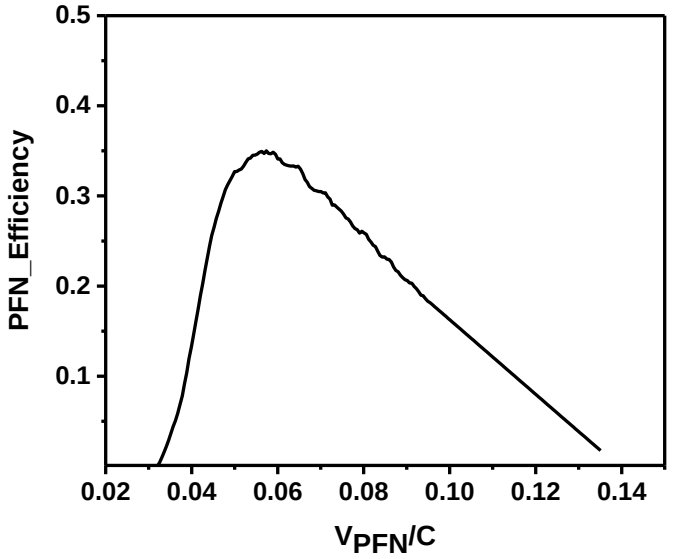

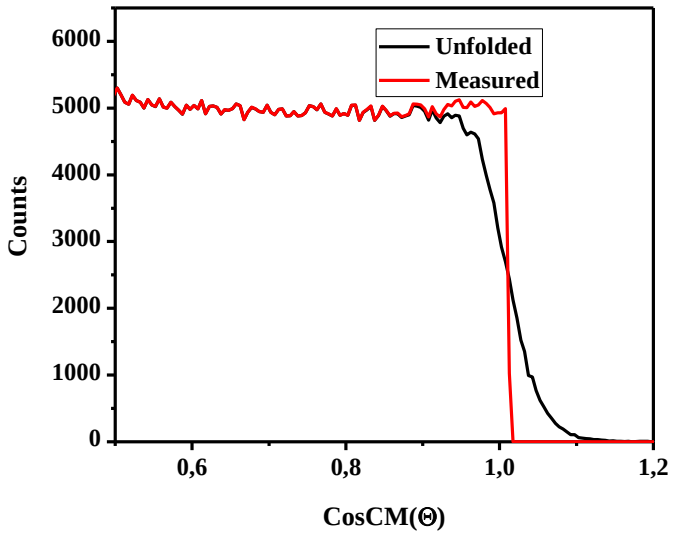

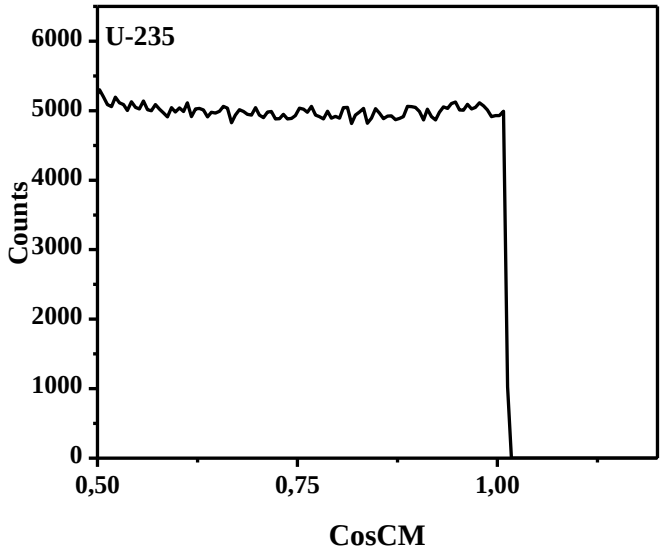

Wonder-2018 October 8-12

14. PFN multiplicity on FF mass evaluation from measured data (assuming isotropic PFN emission in CM)

$$\bar{\nu}(A) = \int_0^{\infty} dV_{LAB} \int_0^{1} d\cos(\Theta) \int_{140}^{220} dTKE \frac{\nu(A, TKE, V_{LAB}, \cos(\Theta) \cdot V_{CM} \cdot (V_{LAB} - V_F \cdot \cos(\Theta))}{V_{LAB}^2 \cdot \varepsilon(V_{LAB})} / \int_0^{\infty} Y(A, TKE) dTKE$$

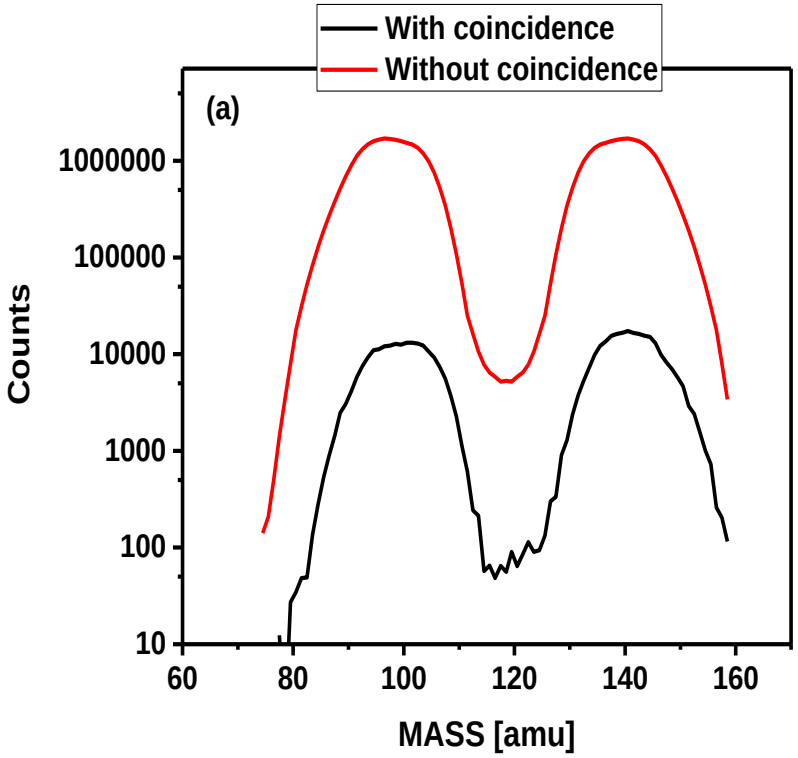

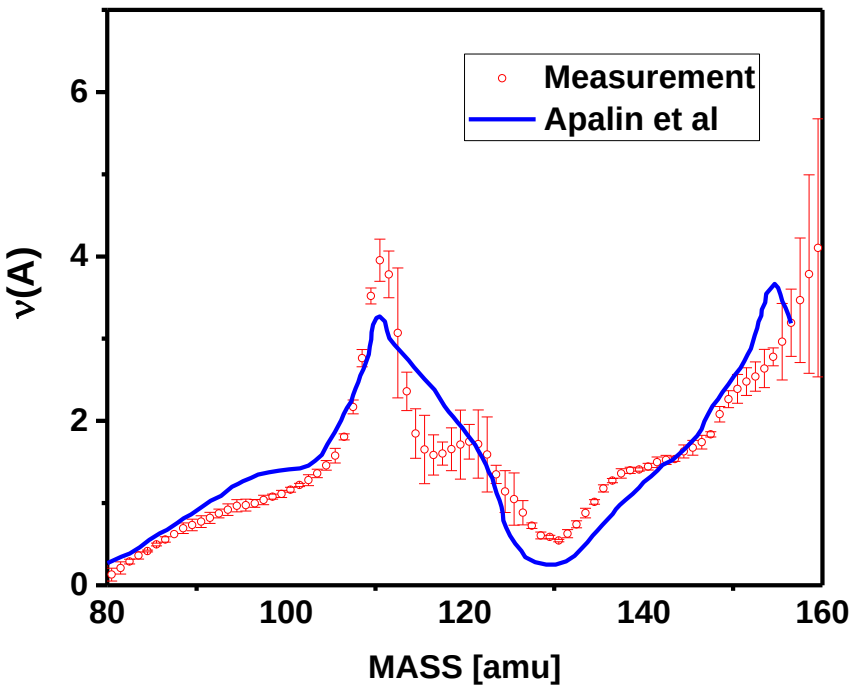

FF mass and Energy values were calculated in iterative procedure taking into account FF recoil after PFN emission according to A. Gavron, Nucl. Instrum. and Meth., 115 (1974) 99

15. PFN multiplicity on FF TKE evaluation from measured data (assuming isotropic PFN emission in CM)

$$\bar{\nu}(TKE) = \int_0^{\infty} dV_{LAB} \int_0^{1} d\cos(\Theta) \int_A dA \frac{\nu(A, TKE, V_{LAB}, \cos(\Theta)) \bullet V_{CM} \bullet (V_{LAB} - V_F \bullet \cos(\Theta))}{\varepsilon(V_{LAB}) \bullet V_{LAB}^2} / \int_0^{\infty} Y(A, TKE) dA$$

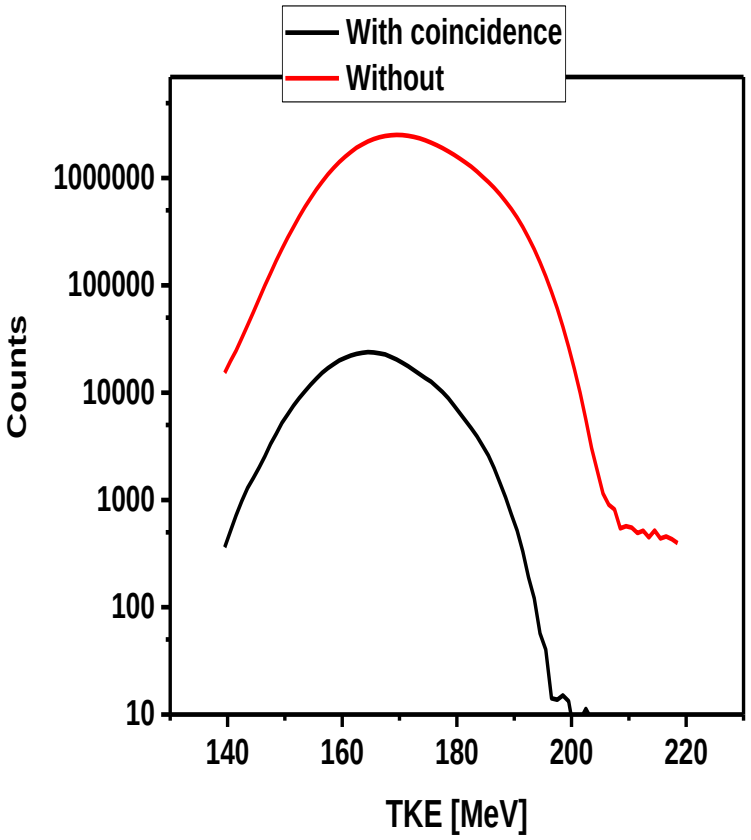

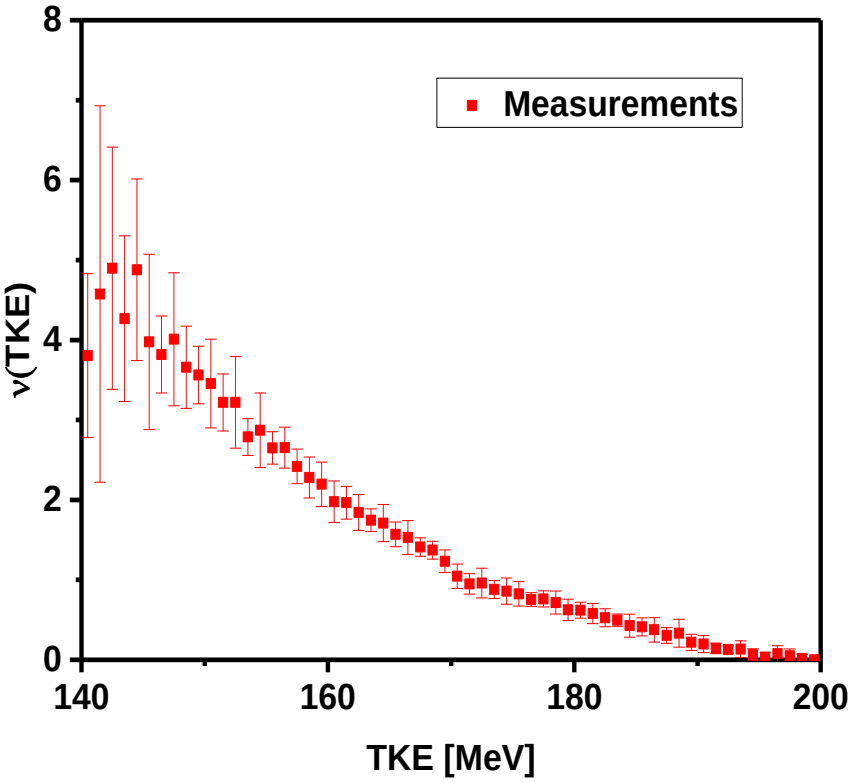

16. Experimental setup and data acquisition system in 252Cf(sf) experiment.

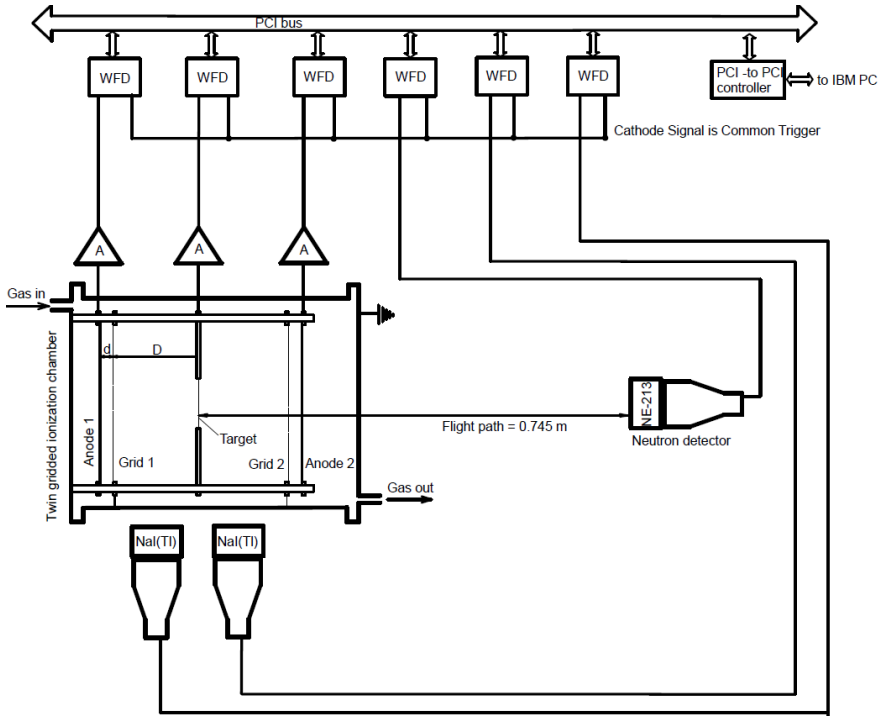

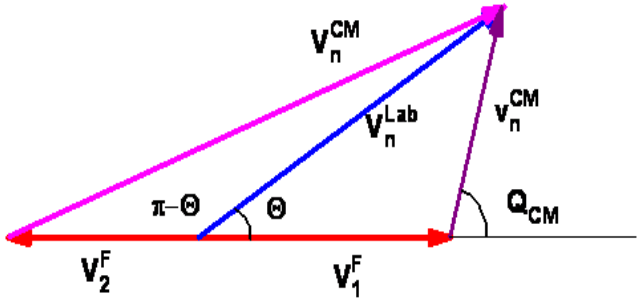

$$\bar{\nu}(A)=\frac{\int_0^{\infty}\nu(A,TKE)Y(A,TKE)dTKE}{\int_0^{\infty}Y(A,TKE)dTKE},\quad \bar{\nu}=\int_0^{\infty}\nu(A,TKE)Y(A,TKE)dTKEdA,\quad 200=\int_0^{\infty}Y(A,TKE)dTKEdA$$

$$\bar{\nu}(TKE)=\frac{\int_0^{\infty}\nu(A,TKE)Y(A,TKE)dA}{\int_0^{\infty}Y(A,TKE)dA},\quad \bar{\nu}=\int_0^{\infty}\nu(A,TKE)Y(A,TKE)dTKEdA,\quad 200=\int_0^{\infty}Y(A,TKE)dTKEdA$$

Adopted from C. Budtz-Jørgensen and H.-H. Knitter, *Nucl. Phys.*, A490, 307(1988) and modified with digital pulse processing apparatus. The only difference to 235U(nth,f) experiment was increase in sampling frequency of WFD

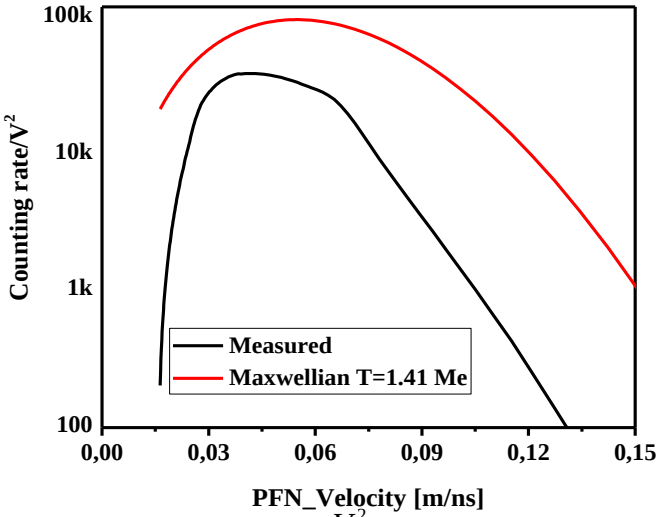

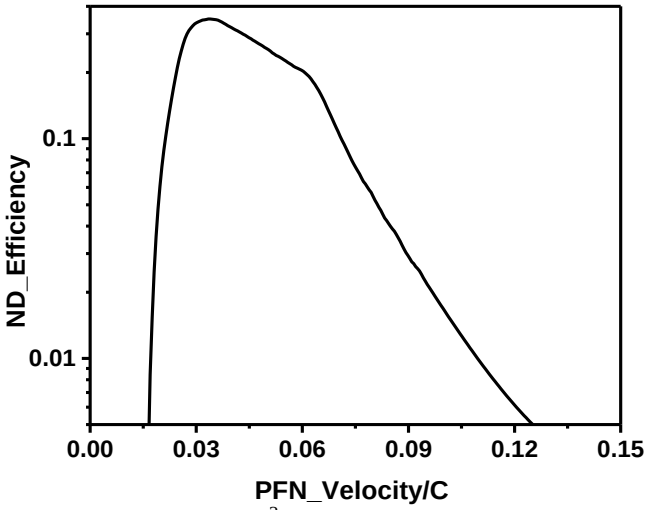

$F(V) = \exp(-\frac{mV^2}{2kT}), \mathrm{kT} = 1.41\,\mathrm{MeV};$ where $M(V) \sim V^2 \exp(-\frac{mV^2}{2kT})$ - Maxwell distributi on

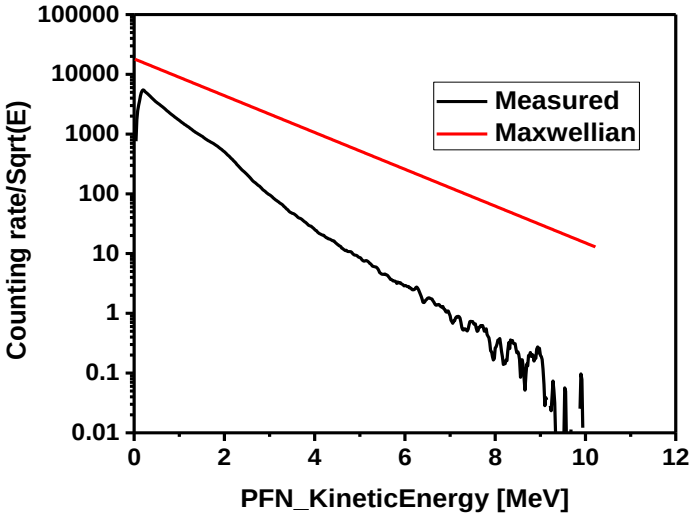

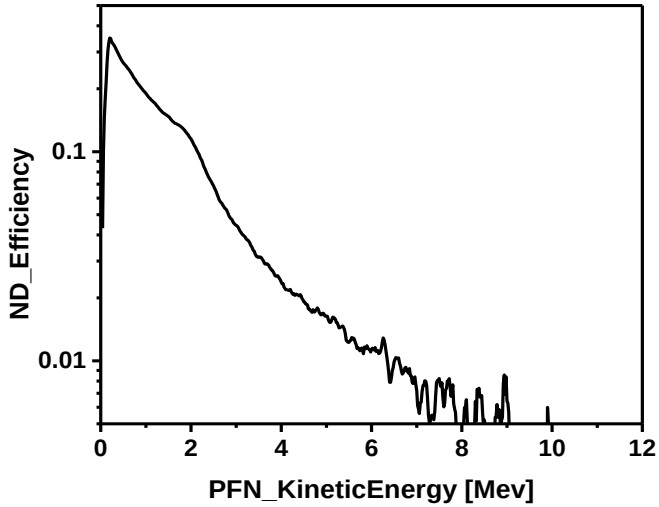

$F(V) = \exp(-\frac{E}{kT}), \mathrm{kT} = 1.41\,\mathrm{MeV};$ where $M(V) \sim \sqrt{E} \cdot \exp(-\frac{E}{kT})$ - Maxwell distributi on

Wonder-2018, October 8-12

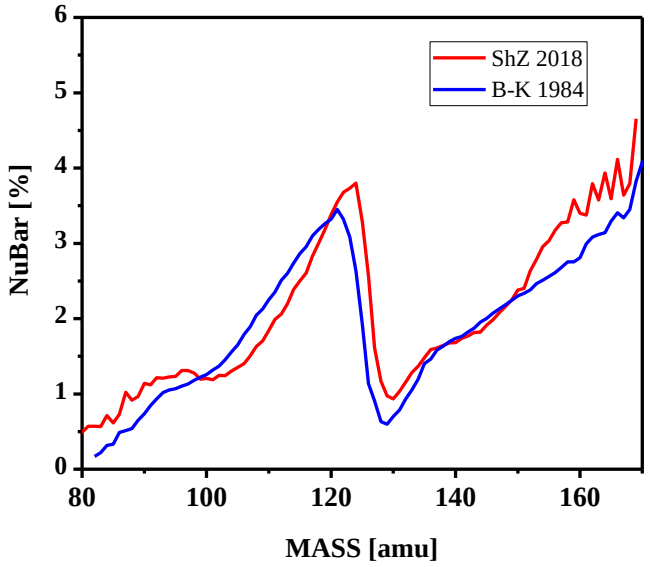

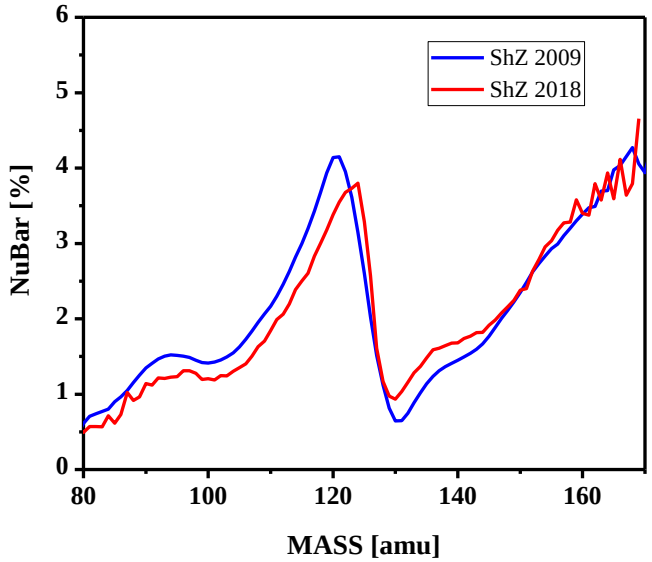

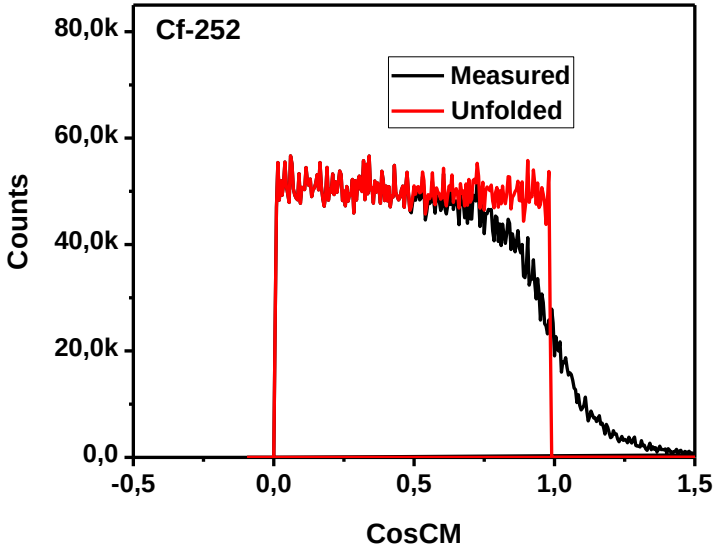

Wonder-2018, October 8-12

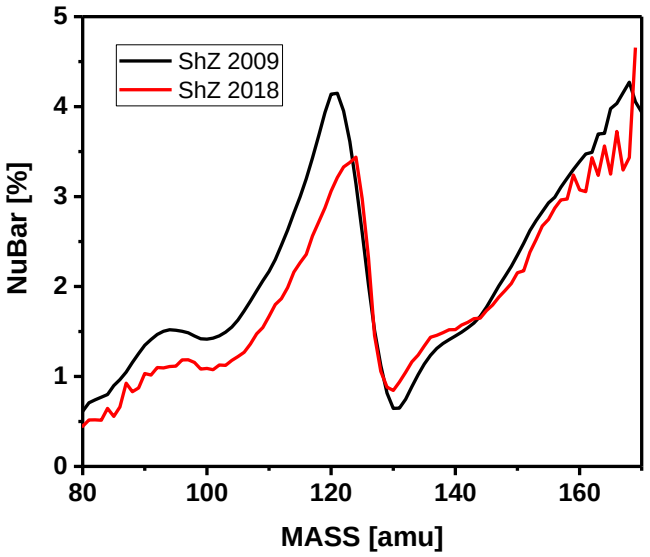

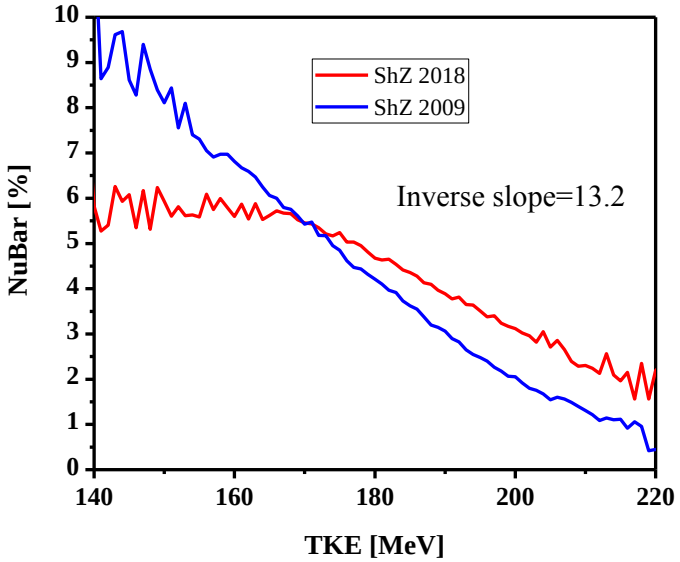

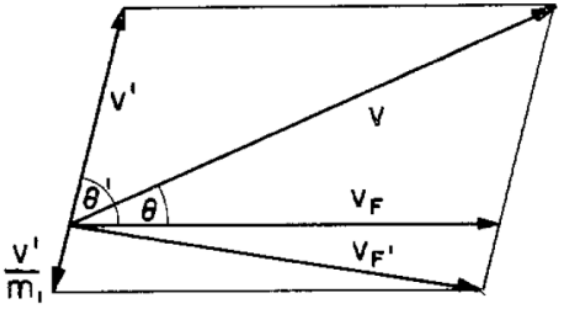

The new analysis have taken into account FF kinetic energy correction due to FF recoil Due to PFN emission

New experimental facility for PFN investigations in Dubna

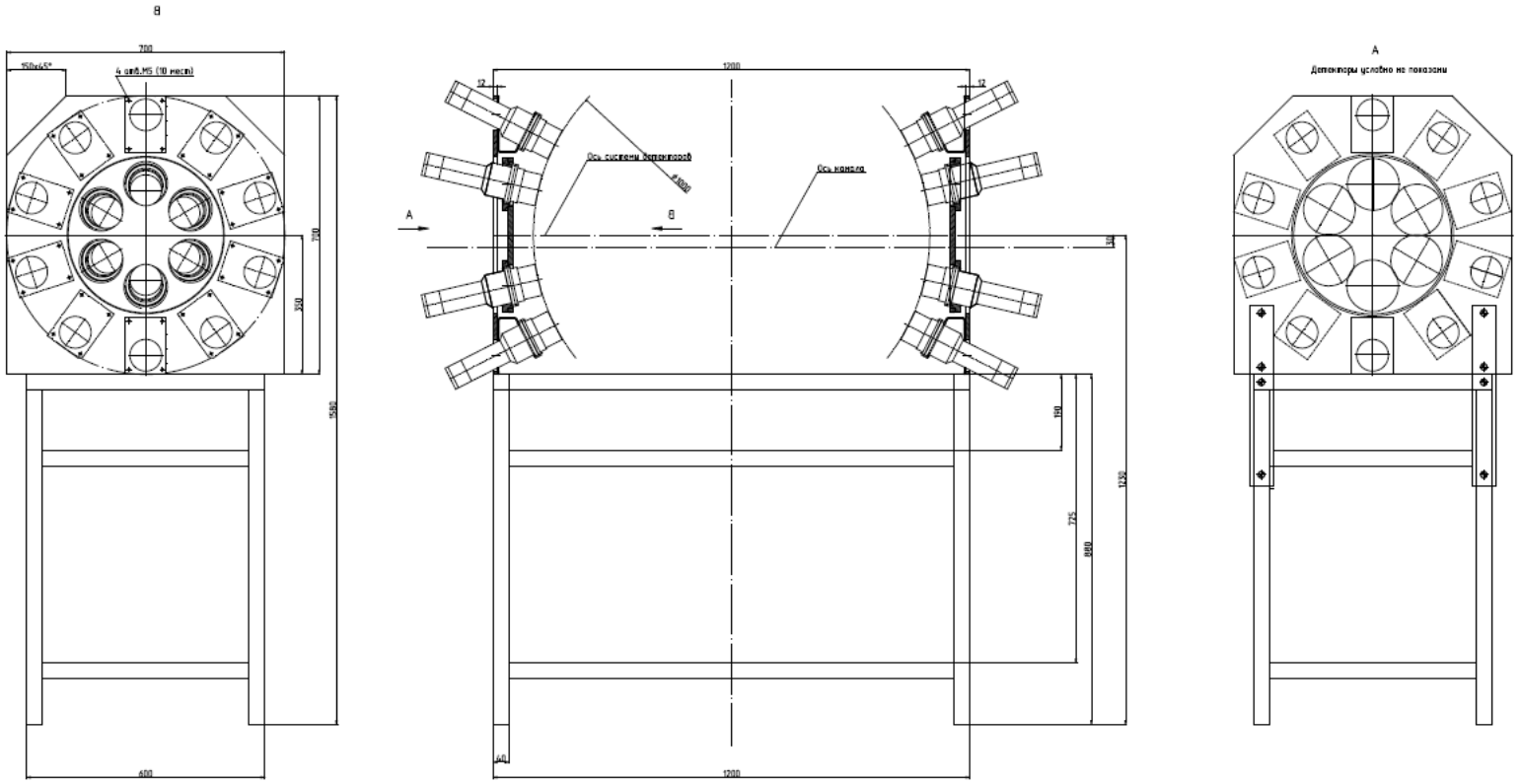

For this new facility new Twin chamber was developed and tested.
Thanks to position sensitivity of the chamber the cosine of angle between Fission axis and PFN can be measured with accuracy better than 0.02

Wonder-2018, October 8-12

Prompt fission neutron investigation

Experimental Results with Fission Fragment Detection (precision)

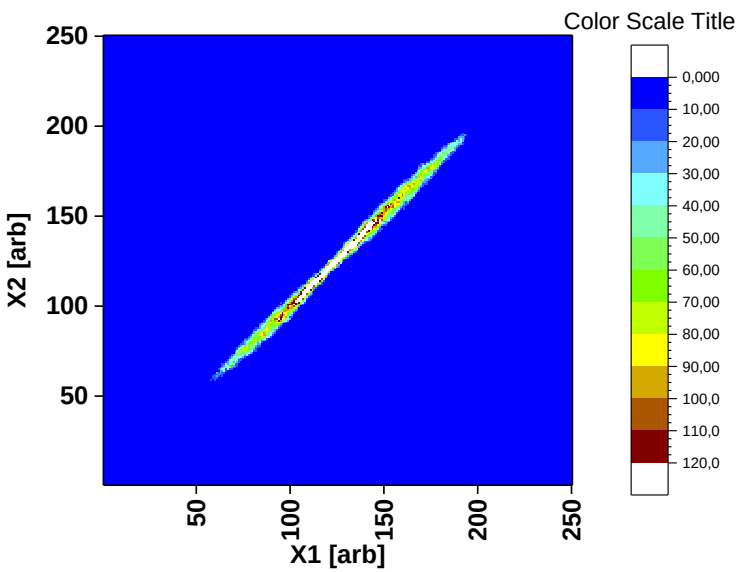

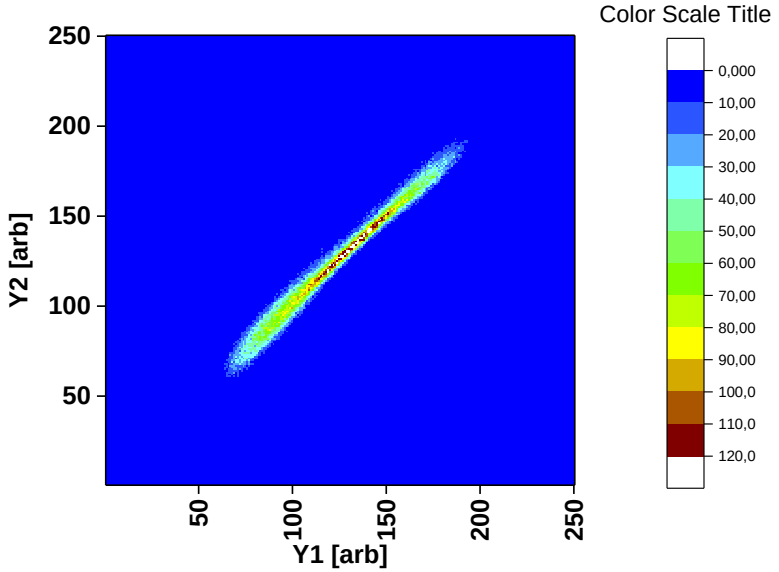

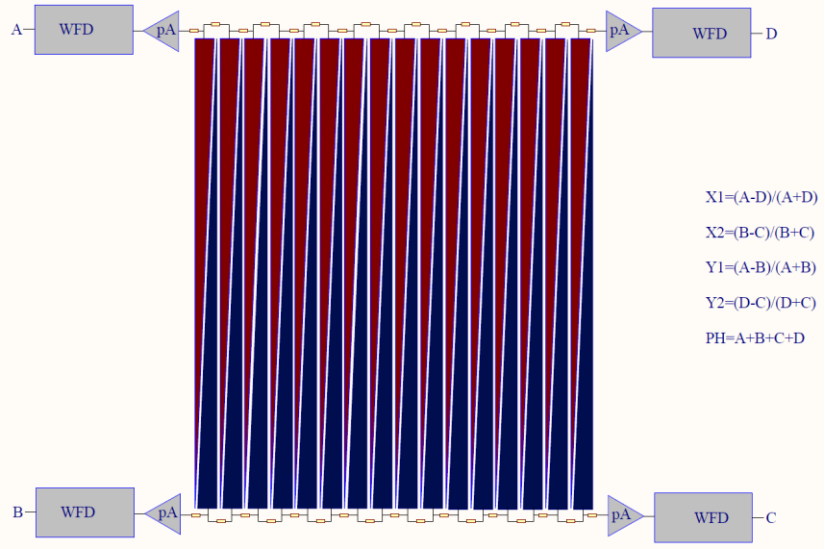

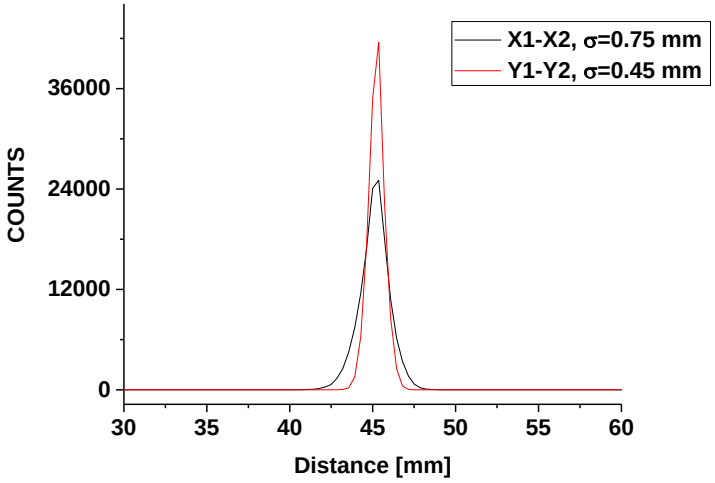

Wonder-2018, October 8-12

14. Conclusions

1. The digital data acquisition system was developed and tested in experiment.
2. The digital pulse processing algorithms was developed and tested both on-line and off-line.
3. The software for PFN multiplicity analysis was revised and some known bugs were removed
4. The result obtained in this work are differ from the literature and it forces us to revise
5. all stage of new development to verify or improve our recent result.

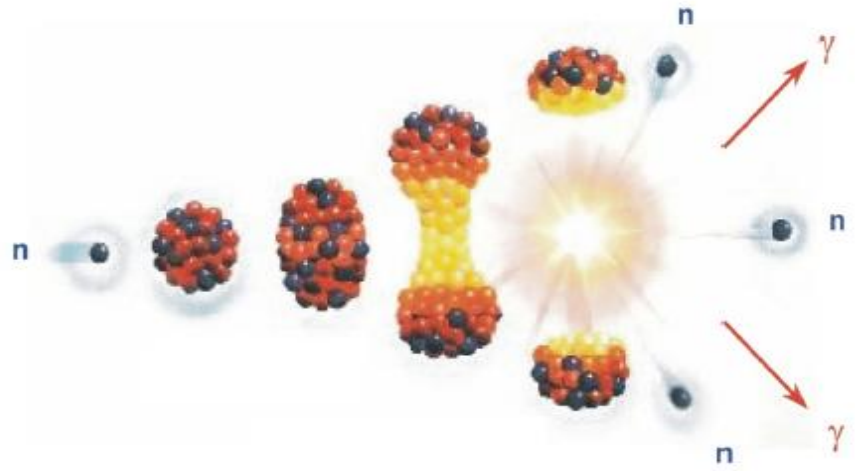

Thank you for your attention ☺

Cf-252

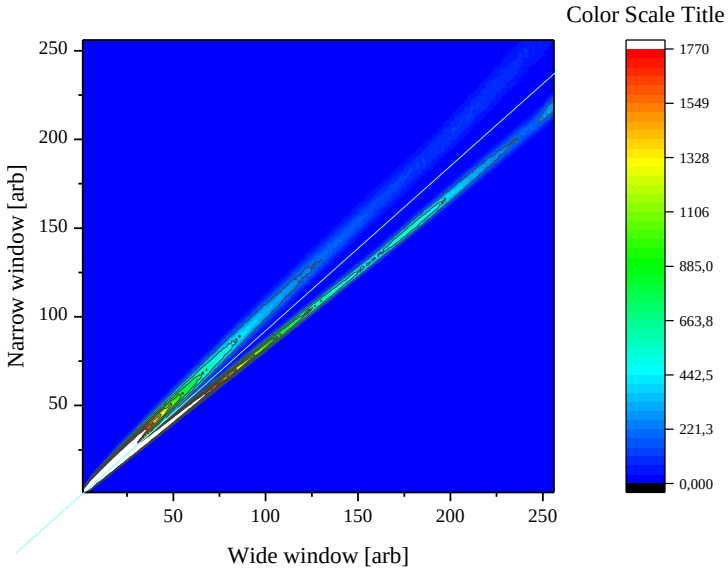
Color Scale Title
Narrow window [arb]
Wide window [arb]
250
200
150
100
50
50
100
150
200
250
1770
1549
1328
1106
885,0
663,8
442,5
221,3
0,000

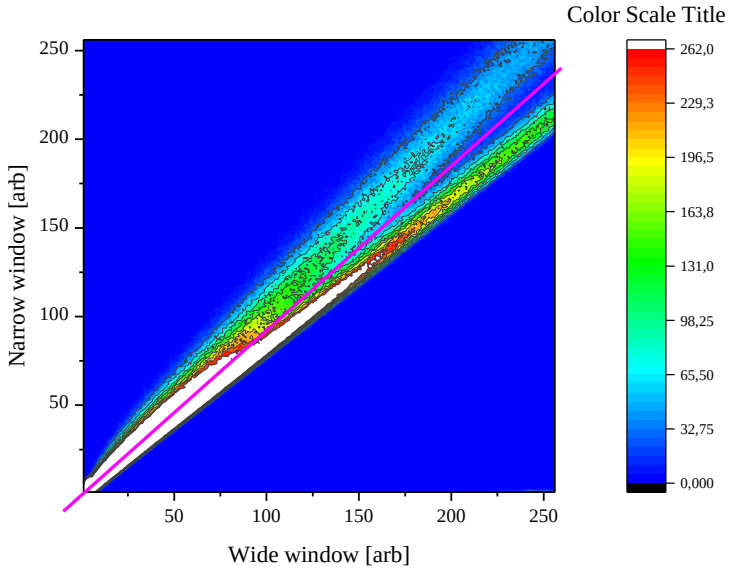
Color Scale Title
Narrow window [arb]
Wide window [arb]
250
200
150
100
50
50
100
150
200
250
262,0
229,3
196,5
163,8
131,0
98,25
65,50
32,75
0,000

U-235

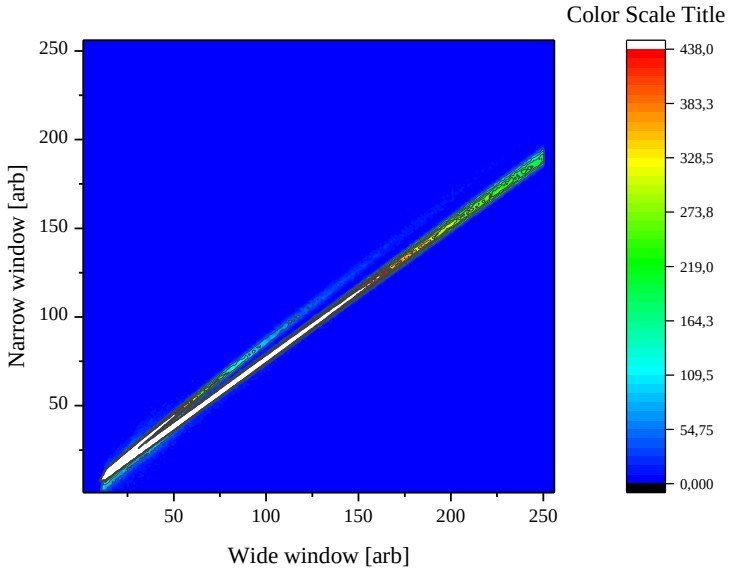
Color Scale Title
Narrow window [arb]
Wide window [arb]
250
200
150
100
50
50
100
150
200
250
438,0
383,3
328,5
273,8
219,0
164,3
109,5
54,75
0,000

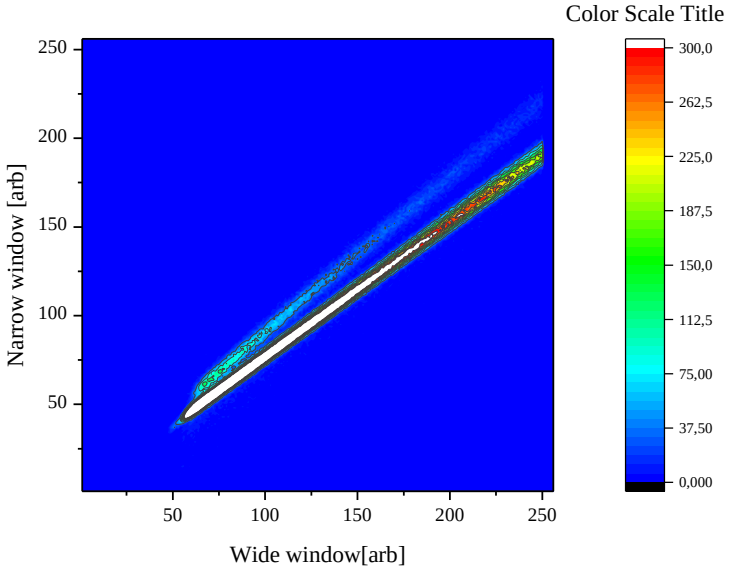
Color Scale Title
Narrow window [arb]
Wide window[arb]
250
200
150
100
50
50
100
150
200
250
300,0
262,5
225,0
187,5
150,0
112,5
75,00
37,50
0,000